

Decomposition of methane hydrates in sand, sandstone, clays, and glass beads

Tsutomu Uchida,¹ Satoshi Takeya,² Evgene M. Chuvilin,³ Ryo Ohmura,² Jiro Nagao,² Vladimir S. Yakushev,⁴ Vladimir A. Istomin,⁴ Hideki Minagawa,² Takao Ebinuma,² and Hideo Narita²

Received 30 August 2003; revised 24 February 2004; accepted 5 March 2004; published 11 May 2004.

[1] Decomposition conditions of methane hydrates in sediments were measured during formation-decomposition cycles. As test sediments, we used silica sand, sandstone, and clays (kaoline and bentonite), which are typical natural materials known as hydrate bearing sediments, and the range of samples cover a range of water saturating abilities. To better understand the results, we also used uniformly sized glass beads. Pore effects on decomposition of these materials were investigated by analyzing the pore-space distributions of the materials and by varying the initial water content of the samples. The results obtained for sand and sandstone samples indicated that the final decomposition temperatures were shifted lower than those for bulk hydrates at the same pressure. Temperature shifts were more negative for smaller initial water contents with the maximum shift being approximately -0.5 K. The results were consistent with those measured for glass beads with nearly the same particle size. For kaoline clays, the shift was at most -1.5 K. We conclude that the decomposition conditions are mainly affected by the pore sizes. The surface textures and mineral components had less influence on the results. We confirmed that glass beads mimic the effect of sediments for sand, sandstone, and kaoline clays, which have little to no swelling when put in contact with water. On the other hand, for bentonite particles, the results indicated that methane hydrates formed not only between the particles but also in the interlayers. A thermodynamic promoting effect was found for dilute bentonite solutions, although the positive decomposition-temperature shift was at most $+0.5$ K. **INDEX TERMS:** 1823 Hydrology: Frozen ground; 3322 Meteorology and Atmospheric Dynamics: Land/atmosphere interactions; 3339 Meteorology and Atmospheric Dynamics: Ocean/atmosphere interactions (0312, 4504); 4524 Oceanography: Physical: Fine structure and microstructure; **KEYWORDS:** methane hydrate, decomposition temperature shift, pore space distribution, artificial fine particle, water content

Citation: Uchida, T., S. Takeya, E. M. Chuvilin, R. Ohmura, J. Nagao, V. S. Yakushev, V. A. Istomin, H. Minagawa, T. Ebinuma, and H. Narita (2004), Decomposition of methane hydrates in sand, sandstone, clays, and glass beads, *J. Geophys. Res.*, *109*, B05206, doi:10.1029/2003JB002771.

1. Introduction

[2] Knowing the equilibrium conditions of natural gas hydrates is important for estimating the total amount of gas in gas-hydrate fields, finding the location of the bottom of the hydrate stability zone (BGHS), and determining the feasibility of extracting natural gas from gas-hydrate fields. However, even if a bottom-simulating reflector (BSR) is

used in the field to estimate the depth and amount of natural gas hydrates, laboratory experiments on the equilibrium conditions are needed to calibrate the BSR.

[3] The equilibrium condition of gas hydrates in sediments, which is referred to here as the decomposition temperature at a given pressure, is affected by the gas and water composition. As an example, the decomposition temperatures of methane-propane ($\text{CH}_4 - \text{C}_3\text{H}_8$) mixed gas hydrates are higher than that of pure CH_4 hydrate [Van der Waals and Platteeuw, 1959; Sloan, 1998]. Also, the decomposition temperature of methane hydrates in NaCl solution is lower than that in pure CH_4 hydrate [Sloan, 1998]. These effects of gas and water compositions have been well studied and provide enough knowledge to estimate the BGHS in sediments under the seafloor and permafrost. There is some evidence, however, that shows that the pore and grain size [Clennell *et al.*, 1999], the mineral composition of the particles, and the water content [Yakushev, 1990]

¹Department of Applied Physics, Graduate School of Engineering, Hokkaido University, Sapporo, Japan.

²Institute for Energy Utilization, AIST, Sapporo, Japan.

³Faculty of Geology, Department of Geocryology, Moscow State University, Moscow, Russia.

⁴All Russian Research Institute of Natural Gases (VNIIGAZ), Moscow, Russia.

affect the equilibrium conditions. As an example, there were discrepancies of 30–100 m between the estimated BGHS and the observed BSR in the Ocean Drilling Project (ODP) Leg 164, at Blake Ridge in 1995 [Matsumoto *et al.*, 1996]. The reasons for the depth discrepancies are discussed by Ruppel [1997], who argued that including the effects of the gas composition would make the discrepancies larger and that the effects of the pore water compositions were insufficient. Ruppel concluded that the discrepancies in the inhibition of hydrate formation are most likely explained by the strong capillary forces in fine-grained sediments. Clennell *et al.* [1999] supported these conclusions using their conceptual model.

[4] Various researchers have experimentally studied the effects of porous media on hydrate stability. Makogon [1974, 1981] and Handa and Stupin [1992] showed that the disassociation pressure of CH₄ and C₃H₈ hydrates in small pores of porous media were higher than those without pores. Uchida *et al.* [1999, 2002] examined how the decomposition conditions of hydrates are affected by pores of diameter less than 100 nm. Their results indicated that the magnitude of the inhibition of decomposition conditions in small pores was determined by the reduction of the water activity, which is a measure of the chemical potential normalized by the bulk state. Ostergaard *et al.* [2002] and Anderson *et al.* [2003a, 2003b] compiled experimental studies on hydrate equilibria in artificial porous media and discussed the quantitative effect of fine pores on hydrate stability.

[5] However, it is difficult to directly apply these results to natural conditions due to the complicated physical and chemical properties of the sediment matrix. The majority of marine and terrigenous sediments consist of sand (quartz, feldspar, carbonate, tuff), clay (bentonite or montmorillonite, kaolinite, illite), and organic matter. Carbonates, silicates and other mineral components also play important roles, but many of them affect hydrate formation and decomposition in the same way as sand [e.g., Starobinets and Murogova, 1985]. The role of clay particles on hydrate formation in sediments is highly variable due to their low gas permeability and the varying amounts of water activity in clay pores that depend on the water content. The influence of organic matter on hydrate formation and decomposition is less than that of sands and clays. Although hydrate formation conditions in sands is relatively well known [e.g., Makogon, 1981; Chuvilin *et al.*, 2002], hydrate formation conditions in clays is poorly known. This is attributed to the experimental difficulties of characterizing and working with wet clays. The importance of clay on hydrate formation was found by Yakushev [1990] and Chuvilin *et al.* [2002]. Yakushev [1990], experimentally showed that low water contents of clay inhibited hydrate formation in spite of having good permeability in the unconsolidated clay powder. An increase of the water content resulted in an increase in the hydrate accumulation in the same clay sample. Clennell *et al.* [1999] and Henry *et al.* [1999] proposed detailed models and did thermodynamic calculations of natural gas hydrates in marine sediments. These models are useful not only for understanding hydrate equilibria in natural conditions, but also for interpreting experimental data obtained under complicated and difficult conditions.

[6] In this study, we reveal the factors with the largest effect on CH₄-hydrate equilibria in natural samples (sand, sandstone and clays) and in artificial samples (various sized glass beads). This is the first hydrate study that includes both natural and artificial samples. The natural samples were selected based on particular properties, such as powder/consolidated structures and water saturating abilities. Glass beads with diameters of 20 and 100 μm were used to understand the effects of the surface textures or the mineral compositions on the hydrate stabilities. We did experiments using various water contents in the sample, which allowed us to estimate the conditions under which hydrate grew in large pores, small pores, and in the clay interlayer.

2. Experimental Procedures

[7] In the experiments, we used research-grade methane with average purity of 99.95 mol% (Chiyoda Chemical) and distilled, de-ionized water with an electric conductivity of approximately 5.5×10^{-6} S m⁻¹. For sediment minerals, we included silica sands, sandstones, and clays, which are major mineral components that exist in natural sediments where CH₄ hydrates occur [Clennell *et al.*, 1999]. As a representative type of silica sand sediment, we used Toyoura sand (TS). According to our measurements with a confocal scanning microscope, the diameters ranged from 60 to 150 μm with a mean of about 100.0 μm. Cylindrical samples of Berea sandstone (BS, 40-mm diameter, 10-mm thick) were used as typical sandstones. The main component of Berea sandstone is silica, so this sample was used to determine how the packing of sand grains into sandstone affects the silica sand results. The apparent grain size, according to our micro-focus X-ray CT measurements, ranged from 50 to 200 μm with a mean of about 115.6 μm. The porosity of the BS sample was measured using a mercury porosimeter to be approximately 17 vol%. For the clays, we chose two types with different water absorption characteristics; kaoline (KA) absorbs the smaller amount of water because the major mineral, kaolinite, has only a narrow space between the clay molecular layers for water adsorption, whereas bentonite (BE) absorbs the larger amount of water due to the high swelling property of the major mineral, montmorillonite. Also, the specific area of bentonite particles was much greater than that of kaoline. The clay samples were purchased from Kishida Chemical Co. (300 mesh). The clay particle sizes were estimated using confocal scanning microscopy. For the KA samples, the diameters ranged from less than 0.1 to 9 μm with an average diameter of about 4.0 μm, whereas the diameters of the BE samples ranged from less than 0.1 to 5 μm with an average value of about 2.3 μm. We compared the results from the clay samples with results from similar clay samples from Russia [Chuvilin *et al.*, 2002]. The Russian samples are denoted RUS_KA and RUS_BE.

[8] Glass beads (GB) of uniform diameter with either a diameter of 20 μm, hereafter denoted as 20GB, and 100 μm, hereafter 100GB, were also used in the experiments. We compared the decomposition conditions of the glass beads with those from similarly sized natural sediments. The main component of GBs was NaO-CaO-SiO₂ (supplied from

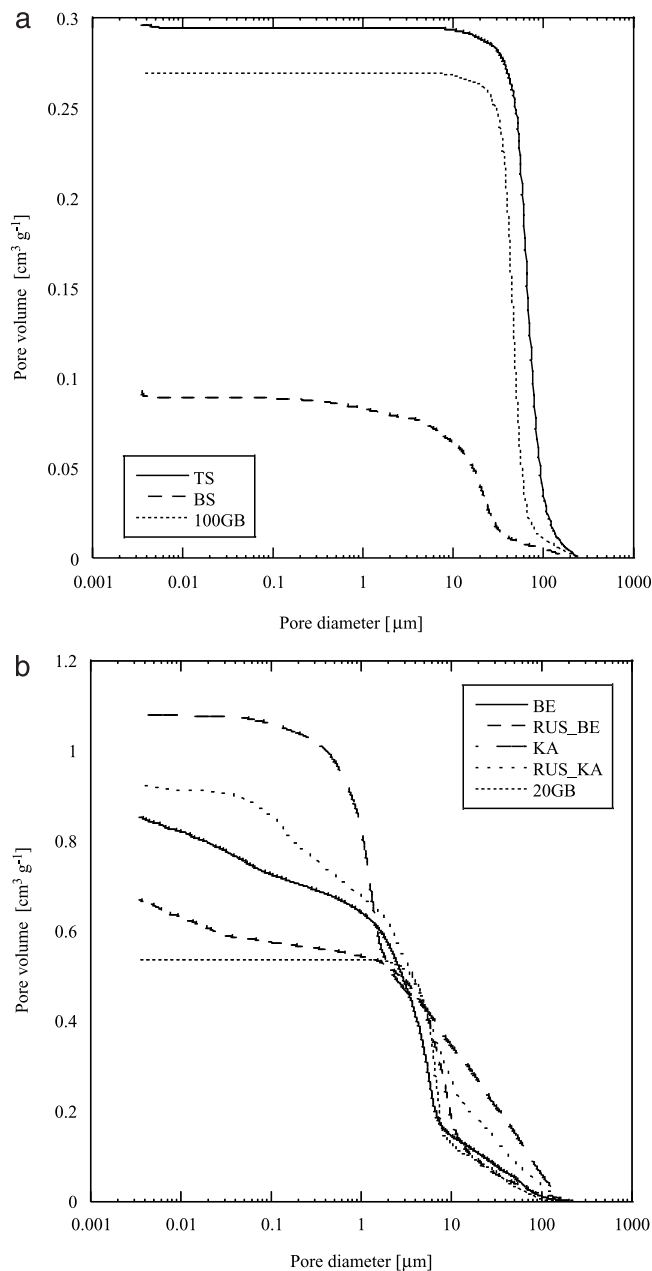


Figure 1. Pore size distributions of dried samples. (a) Silica-sand (TS: solid line) and sandstone (BS, dashed line) with 100- μm diameter glass beads (100GB: dotted line). (b) Kaoline (KA, dashed line; RUS_KA, dotted line) and bentonite (BE, solid; RUS_BE, dashed line) with 20- μm glass beads (20GB, fine dotted line).

Union Co., Ltd.). These comparisons mainly aimed to determine the effects of surface textures on the hydrate equilibria.

[9] The distributions of pore volume and the mode pore diameter for each dry sample were measured using a mercury porosimeter (PoreMaster 60-GT, Quantachrome). Because most of the samples were powder, we measured each sample several times, and confirmed that the reproducibility of the measurements was consistent with the experimental uncertainties. The measured pore diameter distributions are shown in Figure 1 and the physical properties of each sample are listed in Table 1.

[10] The usual sample preparation procedure was to mix the porous medium and pure water at a fixed mass ratio. However, when the low water concentration sample was prepared for BE and KA, the dry samples were first mixed with fine powdered ice at a temperature below 273 K to make the water distribution more uniform. Also, for some experiments at lower water contents, the dry samples were stored in a saturated water vapor condition for several days during which the samples absorbed a significant amount of water. We controlled the water content by controlling the duration of storage. The water content for each sample was estimated using the weight of water in the sample and assuming that the water was uniformly distributed in the sample.

[11] The variation of water content in the samples is expressed by one of two parameters; for clays, we used the volumetric water content λ_w , whereas for sand, sandstone, and glass beads, we used the pore water saturation ratio S_w . The volumetric water content λ_w was determined using the volume ratio of water to the porous material as

$$\lambda_w = (V_w / (V_b + V_w)) * 100, \quad (1)$$

where $V_w = m_w / \rho_w$ is the water volume in the sample, m_w is the mass of added water, $\rho_w = 1 \text{ g cm}^{-3}$ is the density of water in the pore (assumed to be the same as that of bulk water), and $V_b = m_b / \rho_b$ is the bulk volume of dry porous media. Here, m_b is the mass of the porous media and the bulk density ρ_b was measured using a mercury porosimeter (see Table 1). The uncertainties of λ_w were estimated to be approximately 12% for KA and 7% for BE (Table 2). The water content of KA samples were varied from 3 to 24 vol%; for the BE experiments, we measured the equilibrium conditions over a range of λ_w of up to 97 vol%. The wide range of λ_w allowed us to investigate the interesting phenomena of bentonite acting as a promoter of hydrate formation, which was first reported by *Cha et al.* [1988]. To investigate the effects of the water content on the phase

Table 1. Physical Properties for Each Dry Sample According to Porosimeter Measurements

Sample	Mean particle diameter μm	Mode pore diameter d_p μm	Specific pore volume v_p $\text{cm}^3 \text{g}^{-1}$	Bulk density ρ_b g cm^{-3}	Specific porosity $\rho_p = v_p^* \rho_b$
100GB	100.0	44	0.26	1.5	0.38
20GB	20.0	7.5	0.48	1.1	0.51
TS	100.0	68	0.28	1.5	0.41
BS	115.6	22	0.08	2.0	0.17
KA	4.0	1.5	1.2	0.59	0.70
RUS_KA	2.5 ^a	7.1	0.80	0.81	0.63
BE	2.3	5.6	0.79	0.80	0.63
RUS_BE	<1.0 ^a	8.3	0.67	0.90	0.60

^aEstimated from the table by *Chuvilin et al.* [2002].

Table 2. Experimental Conditions and Results for Each Run

RUN Number	λ_{115} vol%	$\delta\lambda_{115}$ vol%	S_{115} vol%	δS_{115} vol%	d_{max} μm	P_d MPa	T_d K	ΔT K	$\delta\Delta T$ K
20GB01	7.0	0.6	14.7	1.9	4.7	6.92	282.1	-0.8	0.3
20GB02	7.0	.6	14.7	1.9	4.7	4.69	278.2	-0.7	0.6
20GB03	4.4	0.4	9.1	1.2	4.0	6.81	282.1	-0.6	0.3
20GB04	19.2	1.5	46.7	6.1	6.7	6.31	281.6	-0.3	0.6
20GB05	9.5	0.8	20.6	2.7	5.3	6.8	281.9	-0.8	0.3
20GB06	15.9	1.3	37.1	4.8	6.3	6.74	282.2	-0.4	0.3
20GB07	12.5	1.0	28.1	3.7	5.8	6.23	280.9	-0.9	0.3
20GB08	26.3	2.1	70.2	9.1	8.0	4.72	278.95	0	0.3
20GB08	26.3	2.1	70.2	9.1	8.0	4.46	277.9	-0.4	0.3
20GB09	2.7	0.2	5.4	0.7	3.4	5.43	278.08	-2.3	0.3
20GB10	9.8	0.8	21.5	2.8	5.4	5.65	279.9	-0.9	0.3
20GB11	17.3	1.4	41.1	5.3	6.4	5.21	279.78	-0.2	0.3
20GB12	23.5	1.9	60.2	7.8	7.3	5.15	279.83	0	0.3
100GB01	3.1	0.2	11.5	0.6	33.5	3	274.45	0.1	0.3
100GB02	3.1	0.2	11.5	0.6	33.5	4.69	278.92	0.1	0.3
100GB03	5.5	0.3	21.2	2.8	38.3	4.83	279	-0.2	0.3
100GB04	8.1	0.4	31.9	1.6	41.3	4.7	278.9	0	0.3
100GB05	12.4	0.6	51.2	2.6	46.4	4.61	278.7	0	0.3
100GB06	1.4	0.1	5.0	0.3	26.0	4.79	278.8	-0.3	0.3
TS01	19.1	1.2	79.5	6.4	87.8	7.05	283.1	0	0.3
TS02	5.7	0.4	20.4	1.6	53.0	6.55	281.9	-0.3	0.3
TS03	1.1	0.1	3.6	0.3	26.0	6.52	281.9	-0.4	0.3
TS04	7.4	0.5	26.9	2.2	56.5	6.4	282.1	-0.1	0.3
TS05	10.5	0.7	39.7	3.2	62.5	6.29	281.9	0	0.3
BS01	1.0	<0.1	11.5	1.3	1.3	4.71	279	0.1	0.3
BS02	0.8	<0.1	9.5	1.1	0.9	4.76	278.6	-0.4	0.3
BS03	1.8	0.1	21.6	2.4	6.0	4.8	279.15	0	0.3
BS03	1.8	0.1	21.6	2.4	6.0	4.79	278.8	-0.3	0.3
BS04	1.5	<0.1	17.6	1.9	4.6	4.61	278.45	-0.2	0.3
BS05	4.8	0.1	58.8	6.5	20.8	6.65	282.8	0.3	0.6
BS06	4.8	0.1	59.3	6.5	21.0	4.87	279.4	0.2	0.3
BS07	4.9	0.2	60.8	6.7	21.4	4.76	279.2	0.2	0.3
BS08	4.8	0.1	58.8	6.5	20.7	6.44	282	-0.2	0.4
BE01	24.8	1.7				3.89	276.7	-0.3	0.3
BE02	76.1	5.3				6.34	281.1	-0.9	0.3
BE02	76.1	5.3				6.72	282.5	-0.1	0.3
BE03	76.1	5.3				6.78	282.8	0.1	0.3
BE04	76.1	5.3				4.7	278.8	0	0.3
BE04	76.1	5.3				5.49	280.5	-0.1	0.3
BE05	76.1	5.3				6.1	281.4	-0.2	0.3
BE06	16.3	1.1				6.35	280.9	-1.1	0.3
BE07	19.0	1.3				6.23	280.4	-1.4	0.3
BE08	76.1	5.3				7.16	282.9	-0.3	0.3
BE09	43.5	3.1				6.44	281.9	-0.2	0.3
BE10	84.1	5.9				6.88	283	0.2	0.3
BE11	84.1	5.9				6.95	283	0.1	0.3
BE12	51.4	3.6				7.12	282.9	-0.3	0.4
BE13	80.9	5.7				6.82	282.7	0	0.3
BE14	25.2	1.8				5.46	280	-0.4	0.3
BE15	25.2	1.8				4.61	278.2	-0.5	0.3
BE16	66.3	4.6				5.44	280.5	0.1	0.3
BE17	88.1	6.2				5.49	280.7	0.2	0.3
BE18	91.3	6.4				5.43	280.8	0.4	0.3
BE19	96.9	6.8				5.41	280.8	0.6	0.3
BE20	10.6	0.7				8.265	284.38	-0.38	0.3
RUBE01	3.7	0.3				6.54	276.1	-6.2	0.4
RUBE02	3.7	0.3				6.35	271.3	-10.7	0.6
RUBE03	17.4	1.2				4.9	278.2	-1.1	0.3
RUBE03	17.4	1.2				5.11	279.6	-0.1	0.3
RUBE04	51.3	3.6				5.48	280.45	0	0.3
RUBE05	34.3	2.4				8.68	284.7	-0.6	0.3
RUBE06	10.5	0.7				6.1	280.4	-1.2	0.3
RUBE06	10.5	0.7				6.07	280.7	-0.8	0.3
KA01	6.6	0.8	5.6	0.7	0.3	6.82	282.2	-0.5	0.3
KA02	6.7	0.8	5.7	0.7	0.3	4.87	279	-0.2	0.3
KA03	13.3	1.6	12.1	1.5	0.6	6.83	282.3	-0.5	0.3
KA04	3.4	0.4	2.8	0.3	0.1	6.56	281	-1.3	0.3
KA05	3.4	0.4	2.8	0.3	0.1	6.54	280.9	-1.4	0.3
KA06	20.3	2.4	20.2	2.4	0.9	6.84	282.6	-0.2	0.3
RUKA01	9.7	1.2	12.6	1.5	0.2	6.72	281.7	-0.9	0.3
RUKA02	13.7	1.7	18.8	2.3	0.3	6.98	282.5	-0.5	0.3
RUKA03	13.7	1.7	18.7	2.3	0.4	5.72	280.7	-0.2	0.3
RUKA03	13.7	1.7	18.7	2.3	0.4	4.85	278	-1.2	0.6

Table 2. (continued)

RUN Number	λ_{15} , vol%	$\delta\lambda_{15}$, vol%	S_{15} , vol%	δS_{15} , vol%	d_{max} , μm	P_d , MPa	T_d , K	ΔT , K	$\delta\Delta T$, K
RUKA04	18.4	2.2	26.7	3.2	1.0	5.7	280.8	-0.1	0.3
RUKA05	20.9	2.5	31.2	3.7	1.7	5.67	280.9	0.1	0.3
RUKA06	24.1	2.9	37.5	4.5	2.5	5.67	281	0.2	0.3

equilibrium conditions for materials with low amounts of water absorption, such as sand, sandstone and glass beads, we calculated S_w as

$$S_w = (V_w/v_p m_b) * 100, \quad (2)$$

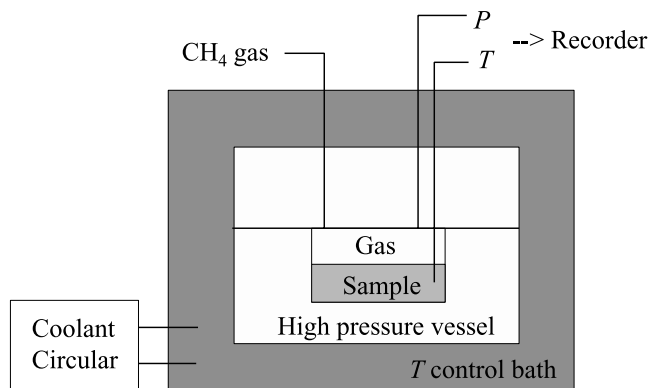
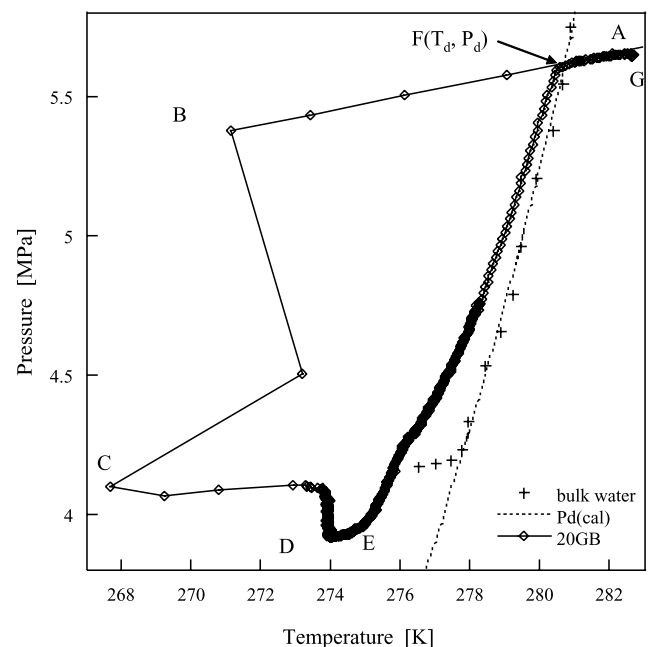
where v_p is the specific pore volume measured with the mercury porosimeter (see Table 1). Here we assumed that the pore size distributions did not change with the addition of water. The uncertainties of S_w varied from approximately 5% for 100GB to 13% for 20GB, depending on the sample.

[12] The equilibrium P - T profiles for methane hydrates in porous media were determined using the simple setup sketched in Figure 2. A high-pressure vessel of about 30-cm³ in volume was connected to a pressure transducer (Kyowa model PHS-100KA, precision ± 20 kPa), a vacuum pump, and a gas source through a manifold. The samples occupied more than 80% of the vessel's volume. A thermocouple of type T was used for the temperature measurements, which was calibrated to a standard thermistor for each experiment. The systematic accuracy of the temperature measurement was estimated to be about ± 0.15 K [Uchida *et al.*, 1999, 2002].

[13] Figure 3 shows a typical pressure and temperature (P - T) curve of the whole experimental procedure. The samples were placed in the high-pressure vessel and then degassed. Gas was then introduced into the vessel by an amount such that at completion of the reaction there would be enough gas left over to stabilize the hydrate (A in Figure 3). The temperature of the vessel was set to well below the experimental condition and maintained by the coolant circulator (Haake model F8-C40). When the hydrate started to form (B), the pressure gradually decreased to the equilibrium one at the set temperature (B to C). Usually we set the temperature to be below the ice point to induce the hydrate nucleation and then we reset the temperature just above the ice point to continue the hydrate growth. The reaction usually finished within one week. After a sufficient amount of hydrate had formed in the sample and the

pressure reduced to equilibrium (D), we gradually raised the temperature of the vessel to measure the decomposition pressure at each temperature (D to E). The rate of temperature increase was about 0.06 K/h. The starting point of each decomposition experiment was a temperature lower and a pressure higher than the three-phase equilibrium conditions of bulk CH₄ hydrates at point D. The significance of point D is that it is the point reached when the pressure drop practically ceased and most of water in the system had already changed into hydrate. When the temperature reached the decomposition value for methane hydrates in the smallest pores (E), the relatively larger pressure increase due to the release of gas from hydrates caused a change of the slope in the P - T diagram. The slope changes gradually when the pore sizes are widely distributed [Uchida *et al.*, 1999, 2002; Wilder *et al.*, 2001; Smith *et al.*, 2002]. When all hydrates in the vessel decompose completely at point F, the pressure increase for a given temperature increase becomes small and thus the slope on P - T diagram becomes small.

[14] Because the unique quadruple point in porous media is difficult to determine, the intersection at point F of the experimental P - T curve (E-F) to the P - T line without any hydrate decomposition (F-G, parallel to line A-B) was

**Figure 2.** Experimental setup.**Figure 3.** P - T curve for the entire experimental procedure (solid line; measured on 20GB) and the graphical method to determine the decomposition condition. The dotted line was calculated using the commercially supplied software (CSMHYD [Sloan, 1998]). P - T curve for the bulk hydrate is shown by crosses as the reference of the experimental reliability.

assumed to be the decomposition pressure P_d and the decomposition temperature T_d as described by *Ostergaard et al.* [2002]. Point F, hereafter the decomposition point, is considered to coincide with the three-phase equilibrium condition of CH₄ hydrates formed in the largest of the pores that were saturated with water at the start of the experiments. To understand the influence of the pores, we then estimated the temperature shift $\Delta T = T_d - T_e$, where T_e is the decomposition temperature of bulk methane hydrate at P_d . We did phase-equilibrium measurements on bulk methane hydrates (“+” in Figure 3) to check the validity of our experimental technique. All experimental conditions and obtained results for each run are listed in Table 2. The uncertainty of the ΔT determination for each run ranged from ± 0.3 K to ± 0.6 K (Table 2).

[15] *Anderson et al.* [2003a] pointed out that the step heating method is more reliable than the continuous heating method used here for isochoric determination of clathrate decomposition conditions in porous media. Thus we made comparison runs with the step heating method using 20GB with the water content of $S_w = 47$ vol%. To approximate the properties of clay samples, which have smaller pores than glass beads, we used 30-nm porous glass, which we had used in a previous study [*Uchida et al.*, 1999, 2002]. The pores of this sample were saturated with water, then we followed the step heating method of *Anderson et al.* [2003a]; the temperature was raised in 0.5 K steps such that sufficient time (between 8 and 94 hours) was allowed following each temperature rise for the system to reach equilibrium. Figure 4a shows the data from both methods for the 20GB samples. The P - T curve from the step heating method (open circles) nearly equals the P - T curve from the continuous heating method (the solid line). The decomposition points estimated from the diagrams are $T_d = 280.3$ K and $P_d = 5.55$ MPa for the step heating, and $T_d = 280.5$ K and $P_d = 5.62$ MPa for the continuous heating. The estimated temperature shifts for the heating curves from both methods are $\Delta T = -0.2$ K. Similarly, the temperature shifts estimated from the decomposition conditions in 30-nm porous glass are -1.0 K and -0.9 K for the step heating method and the continuous method, respectively (Figure 4b). These results indicate that, within the experimental uncertainty, the continuous heating method used in the present study gives the same results as those obtained with step heating.

3. Results and Discussion

3.1. Silica Sand and Sandstone

[16] Silica sand and sandstone are typical components of sediments in which natural gas hydrates are observed to form. Because these minerals (mainly silicate) do not absorb large amounts of water, CH₄ hydrates would form from water existing originally at the spaces between the particles. The pore distribution of TS is similar to that of the uniform-sized glass beads 100GB, which have nearly the same diameter (see Figure 1a). The difference between TS and 100GB may be the surface textures, so a comparison of hydrate equilibria in TS and 100GB will indicate the effect of the surface texture on the equilibrium condition. On the other hand, BS is a consolidated material that has similar mineral components as TS. As shown in Figure 1a, BS has a

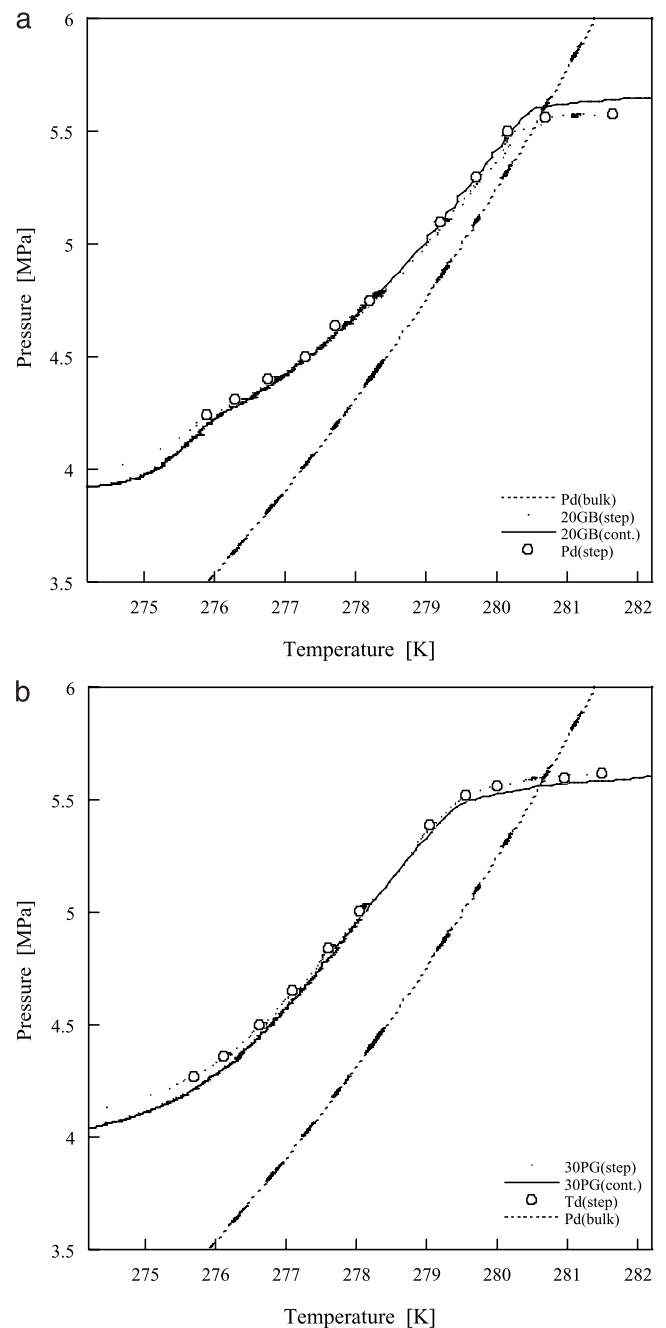


Figure 4. P - T diagrams obtained using the step heating method (dotted line) and the continuous heating (solid line) measured on (a) a 20GB sample and (b) 30-nm porous glass (denoted as 30PG). For the step heating method, each decomposition condition is marked with an open circle. The dotted line was calculated using the commercially supplied software (CSMHYD [*Sloan*, 1998]).

different pore size distribution than TS. In particular, BS has smaller pores and smaller net pore volumes than TS. In the present study, we examined the effects of these differences on the phase equilibrium of CH₄ hydrates under various water content conditions.

[17] The observed temperature shifts ΔT for CH₄ hydrates in TS and BS samples with various S_w are comparable to the

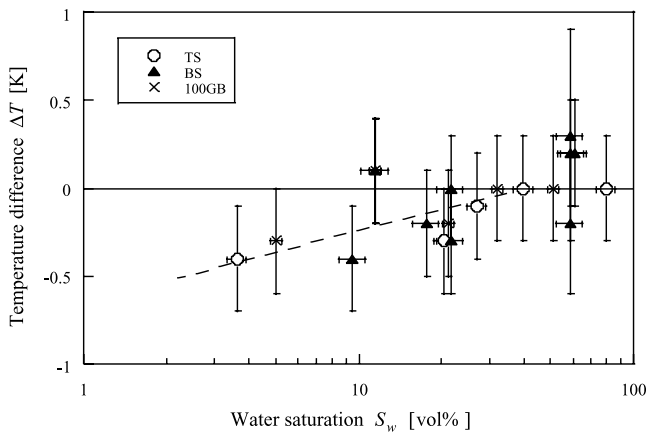


Figure 5. Dependence of ΔT on S_w for silica-sand (TS, open circles) and for sandstone (BS, solid triangles). Data for 100GB are shown as cross marks.

trends found for 100GB (Figure 5). The ordinate shows the temperature shift ΔT and the abscissa shows the water saturation S_w on a logarithmic scale. This figure shows that, at a given pressure, ΔT is negative for S_w below 30 vol% in both porous media. For TS and 100GB samples, S_w has a roughly a logarithmic dependence on ΔT . This result indicates that the three-phase equilibrium conditions of CH₄ hydrates formed between TS particles and also between 100GB particles were at slightly lower temperatures compared with the equilibrium of the bulk phase when the pore space was not initially saturated with water. That is, the pores have an inhibition effect. The data also indicate that the surface textures of the sand particles do not significantly influence the gas hydrate equilibria. Therefore we conclude that glass beads can be a useful test system for studying the equilibrium conditions of hydrate formation in natural sand.

[18] The S_w dependence on ΔT for the Berea sandstone (BS) has a similar trend to that of 100GB, such as the range of ΔT , the maximum S_w providing ΔT to be negative, and the slope of the regression line, and so on, although the trend of the data is less clear than that for TS and 100GB. The reason that the data of BS is similar to that of TS, despite the smaller pores in BS, might be because BS and TS have similar mineral components. Also, the results with TS and 100GB showed that differences of surface texture should not result in significantly different equilibrium conditions. To better understand these findings, we now discuss the formation of hydrate in pores. We assume that the initial distribution of water in the sample is that produced when water is saturated in the smaller pores due to capillary forces. Owing to the relatively small amount of absorption on the silicate, we also assume that there was no change of the pore size distribution caused by the water. CH₄ hydrates would form at the gas-water interface, which we assume are in the largest pores with water saturation (d_{max}). Then the hydrate might grow into the smaller pores during the hydrate formation step, which is the duration between points C and D in Figure 3. At the hydrate decomposition step, the hydrate in the smallest pores would decompose at lowest temperature, which is point E. Therefore the hydrate that decomposed at the final decomposition point (point F) was in the pores of size d_{max} . When the sample was partially

saturated, d_{max} was smaller than the maximum pore size of the sample. Therefore, d_{max} depends on S_w .

[19] In Figure 6, we show the relation between $\Delta T/T_e$ and $1/d_{max}$. This figure shows that $\Delta T/T_e$ for CH₄ hydrates in BS samples has less dependence on $1/d_{max}$ compared with those in TS and 100GB. Samples of 20GB, which are also plotted, have a larger dependence on $1/d_{max}$ than TS, BS, and 100GB. A possible reason for the difference between BS and the other samples is the difficulty of gas hydrate formation in BS compared with other unconsolidated samples. Water might not saturate the smaller pores in BS sample as much as in the other samples because the consolidation of the sand particles might make the pore structures different from those in TS, such as the bottle type for BS and the tube type for TS. This might have led to an underestimate of the influence of $1/d_{max}$ on the temperature shift for BS. The ΔT for the BS sample with $S_w = 12$ vol% (Figure 5) is about zero, which might be due to the decomposition of bulk hydrates formed on the external surface of the BS sample, which can arise from insufficient water absorption and a relatively small amount of hydrate growth into smaller pores.

[20] The temperature shift dependence on maximum pore size is different for the two sizes of glass beads (Figure 6). Although both GB samples have similar trends in that the temperature shifts became more negative with smaller d_{max} values, they do not have the same temperature shift for a given d_{max} . This lack of agreement may have resulted from the two samples having different initial water distributions. Because the pore diameter distributions for GBs were too narrow to produce a gradual water saturation, the water might not occupy the pore spaces but instead exist on the particle surfaces at the initial condition for small S_w sam-

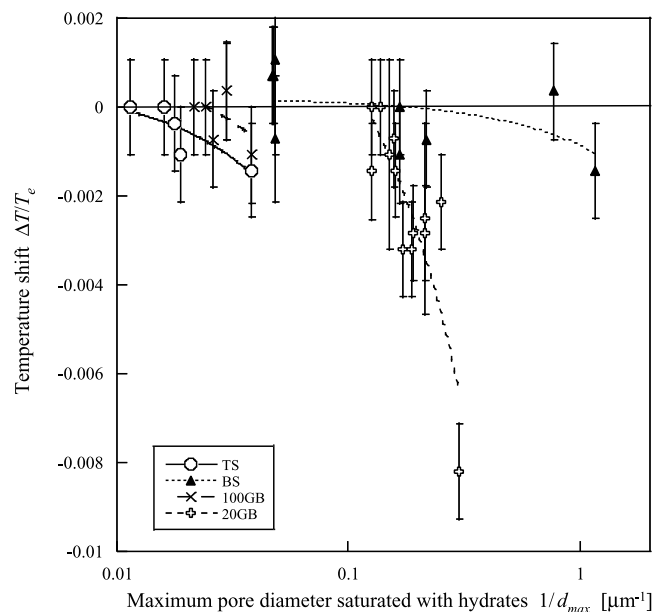


Figure 6. Relation between temperature shift $\Delta T/T_e$ and the maximum pore size saturated with hydrates $1/d_{max}$ for TS, BS, 20GB, and 100GB. T_e is the decomposition temperature of bulk CH₄ hydrate at pressure P_d . Note that the abscissa has a logarithmic scale and each line shows a linear relation.

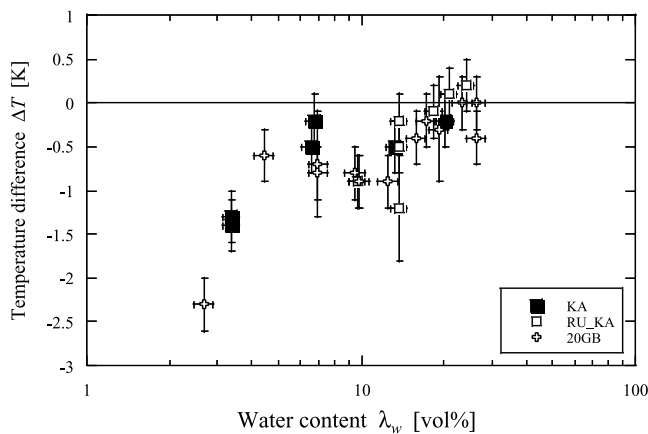


Figure 7. Equilibrium temperature shift ΔT for a range of water contents λ_w for kaoline clays (KA and RUS_KA) and glass spheres (20GB).

ples. In such conditions, hydrates would cover the particle surfaces but not fill the pores. Therefore when the porous matrix is made of unconsolidated coarse particles, the decomposition condition shift should depend on the particle size.

3.2. Kaoline and Bentonite

[21] We also examined the effects of clays on the three-phase equilibrium conditions of CH₄ hydrate. Clays can absorb larger amounts of water than sand or sandstone because they consist of minerals that form stacked molecular plates that can attract water molecules. The plates have a large interlayer surface on which reside loosely held, hydrated cations that interact strongly with water molecules. Therefore in the clay samples, we suspect that water was initially located not only between the grains but also in the interlayers of the mineral grains. To better understand the role of the mineral types, we used two typical clays in the experiments. Of the two, kaoline (KA) has less swelling from water absorption and bentonite (BE) has more swelling. Because clays from different areas have some variation in their composition, we also did experiments using similar clays from Russia. In particular, we used a type labeled RUS_KA, which was mostly kaolinite, and RUS_BE, which was montmorillonite. The pore size distributions of both dried samples were slightly different from those of KA and BE (see Figure 1b).

[22] The temperature shift of the equilibrium conditions of CH₄ hydrates in the KA sample was negative at $\lambda_w < 20$ vol%, and it is most negative at the lowest water contents λ_w (Figure 7). Also, the RUS_KA samples (open squares) have about the same ΔT as the commercially supplied KA sample (solid squares), and both clay samples have a temperature shift trend that is similar to 20GB. The 20GB sample has a similar pore diameter as the clay samples but has less water absorption. Therefore we conclude that hydrate formation in KA samples is inhibited, and for water contents smaller than approximately 20 vol%, CH₄ hydrate in KA samples have an equilibrium temperature that is up to 1.5 K less than that for pure, bulk hydrate. Furthermore, within experimental accuracy, the 20GB samples have the same effect on hydrate equilibrium as the KA samples.

[23] The similarity of the λ_w dependence of ΔT between the KA and 20GB samples might indicate that the absorbed water in the interlayer of KA minerals do not contribute to the hydrate formation. This is expected for the following reason. The distance between the molecular plates of kaolinite is about 1 nm [Smirnov and Bougeard, 1999] and the kaolinite does not swell significantly when it absorbs water. Therefore the water molecules absorbed within the clay particles can form only several molecular layers. This is less than the 30 nm or more that is needed for hydrates to form Uchida et al. [2002]. Thus we assume that the water is absorbed both within particles and between particles in KA sediments, but hydrates form only between particles.

[24] We estimated the size of the largest pores that are saturated with water d_{max} for KA and RUS_KA samples by assuming the pore distribution to be unchanged by the addition of water. The assumption is reasonable because KA and RUS_KA samples have relatively little swelling. The dependence of $1/d_{max}$ on $\Delta T/T_e$ (Figure 8) indicates that the maximum d_{max} that produces a negative ΔT is about 1 μm for both KA and RUS_KA. This figure also shows that the relation between $\Delta T/T_e$ and $1/d_{max}$ for KA is comparable with that for porous glass (PG) but much different than that for 20GB. This may indicate that the particle sizes in KA (several micrometers) are small enough to form hydrates in the pore spaces rather than just the particle surfaces even when S_w is small. However, the dependence of $\Delta T/T_e$ on $1/d_{max}$ in KA is approximately four times larger than that in porous glass. This may be a result of larger interactions between hydrates and kaolinite minerals than those between hydrates and silica glass. The maximum d_{max} here is 1 order larger than that estimated by Uchida et al. [2002]. This

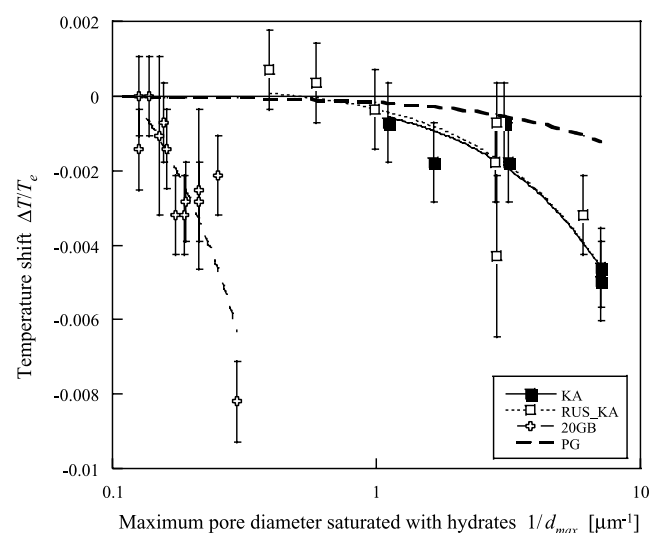


Figure 8. Equilibrium temperature shifts $\Delta T/T_e$ for a range of maximum-sized pores that are saturated with hydrates d_{max} . Samples are kaoline clays (KA and RUS_KA) and glass beads (20GB). Thick dashed line indicates the relation between $\Delta T/T_e$ and $1/d$ for porous glasses obtained in previous work [Uchida et al., 2002]. The fitted curves on the logarithmic scale shown here are straight lines on a linear scale.

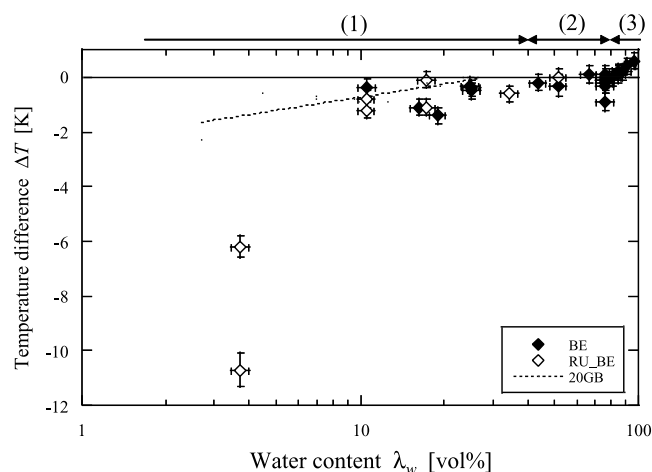


Figure 9. Equilibrium temperature shift ΔT for a range of water contents λ_w for bentonite clays (BE and RU_BE) and glass spheres (20GB). Each number shown on the upper abscissa is a λ_w range discussed in the text.

might have resulted from an overestimate of d_{max} due to a slight change in the pore distributions after adding water.

[25] We conclude that clay particles with relatively little swelling will influence the CH₄ hydrate stability only through their particle sizes. It follows that glass beads with about the same particle size might be a useful test sample for studying the approximate equilibrium conditions of kaoline-rich clay samples, at least within our experimental conditions. This conclusion also supports our argument that the surface textures of the kaoline particles do not significantly influence the gas hydrate equilibria. The similarity of the equilibrium condition shifts of KA and 20GB samples also indicates that the difference of the mineral composition does not affect the hydrate equilibria.

[26] We made similar experiments in the bentonite (BE)-water-CH₄ gas system. Figure 9 shows the temperature shift ΔT in this system for various water contents λ_w . We found no significant difference in ΔT between the commercially supplied BE sample (solid diamonds) and the RU_BE samples (open diamonds). The negative value of ΔT at small λ_w indicates that the equilibrium conditions of CH₄ hydrates in BE samples coincide qualitatively with the general trends observed in other porous materials, such as that in 20GB. However, there appears to be three ranges of λ_w , each with its own functional dependence of ΔT on λ_w : (1) $\lambda_w < 40$ vol%, (2) $40 \text{ vol}\% < \lambda_w < 80$ vol%, and (3) $\lambda_w > 80$ vol%.

[27] In the range of $\lambda_w < 40$ vol%, ΔT is increasingly negative as λ_w decreases. We also found that there were two decomposition points for the same λ_w condition. These points were usually identified through the two steps in the P - T curve as shown in Figure 10. The ΔT value with the smaller magnitude, point F_2 in Figure 10, roughly equals the value for the 20GB samples. These points likely arise from the decomposition of the hydrates that formed between BE particles, which coincide with those observed in KA samples. This interpretation of the F_2 point is supported by the similarity of the pore space distributions of BE, RU_BE, and 20GB for pores larger than 3 μm (Figure 1b).

[28] It follows that the larger ΔT values, that is, point F_1 in Figure 10 and data lower than dotted line observed for

λ_w smaller than 40 vol% in Figure 9, are due to a decomposition phenomenon of CH₄ hydrates that has a greater inhibition effect than that from the pores. A possible explanation is that this ΔT is due to hydrate formed in the interlayers of swelled bentonite minerals. Such a hydrate might form from CH₄ gas and water that are absorbed between the molecular plates of montmorillonite. This clay-CH₄ hydrate intercalate was studied using computer simulations [e.g., Park and Sposito, 2003] and was confirmed by X-ray diffraction [Guggenheim and Koster van Groos, 2003]. Structural analysis of X-ray diffraction data indicated that the interlayer hydrate had a one-unit cell layer structure between the molecular plates of montmorillonite, which was similar to that of bulk CH₄ hydrate.

[29] In addition, Guggenheim and Koster van Groos [2003] showed the equilibrium conditions of the interlayer hydrate to be shifted near $\Delta T = -1$ K. Although they did not provide the quantitative information of water contents, they mentioned that the starting material contained sufficient water. On the basis of the results obtained in the present study, the temperature shift of $\Delta T = -1$ K indicated the water content of λ_w to be near 40 vol% for the interlayer hydrate. This might be similar to the “sufficient” water content. The above authors also mentioned that interlayer hydrates are relatively difficult to form and this difficulty is strongly dependent on the water content. This agrees with the findings here.

[30] Using the relation between ΔT and the pore diameter of porous glasses [Uchida et al., 2002], we estimated the apparent pore space for the interlayer hydrates in each equilibrium condition. For example, ΔT in the BE samples

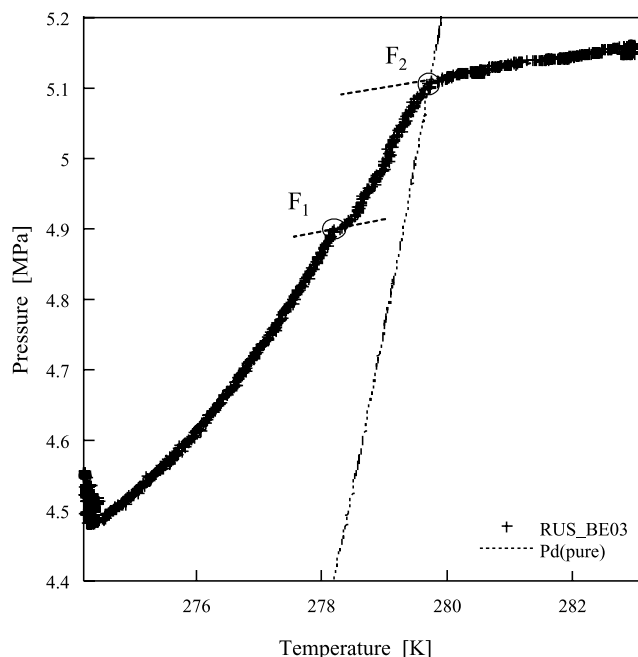


Figure 10. Typical P - T curve for BE sample (run RUS_BE03) with two-step decomposition. F_1 and F_2 mark the steps. The decomposition conditions in each step are determined as the intersection of the P - T curve and the dashed lines. The dotted line was calculated using commercially supplied software (CSMHYD [Sloan, 1998]).

is approximately -8 K at λ_w equal to approximately 4 vol%. This temperature shift coincides with the effect predicted for small pores of approximately 6 nm. This value is larger than the 2.2-nm distance between plates estimated from X-ray measurements [Guggenheim and Koster van Groos, 2003] hence the water or hydrate accumulation in the sample might have caused the distance between the plates to increase from 2.2 to about 6 nm.

[31] In the range of λ_w between 40 and 80 vol%, ΔT is roughly zero. This might be caused by the impermeability of CH₄ gas into the sample under this range of water content. In this range, CH₄ hydrates likely form from the water on the surface of the clay sample and thus grow as bulk CH₄ hydrate.

[32] In the range of λ_w above 80 vol%, the sample was a solution that contains BE particles. Some experimental results indicated slightly negative value of ΔT , which may have resulted from an inhibition effect from ions that dissolved from bentonite minerals. ΔT becomes slightly positive as λ_w increases. This ‘thermodynamic promoting’ phenomenon was first reported by Cha *et al.* [1988] for a solution that contained bentonite. They observed ΔT values as large as $+15$ K at a given pressure. Later, some researchers made efforts to reproduce this strong promoting phenomenon but they reported only a slight promoting effect [Ouar *et al.*, 1992] or practically no effect [e.g., Englezos and Hall, 1994; Lee *et al.*, 2002]. The thermodynamic promoting effect was also studied using computer simulations of CH₄ hydrates in the presence of montmorillonite surfaces [Park and Sposito, 2003]. The value of ΔT measured in the present study was at most 0.5 K, which was much smaller than those observed by Cha *et al.* [1988]; nevertheless, our results appeared to support the thermodynamic promoting effect. As was described by Kotkoskie *et al.* [1992], the equilibrium conditions of gas hydrates in bentonite-rich clay are determined by the competition between the promoting effect of the bentonite minerals and the inhibiting effect of the electrolytes dissolved into solutions from the minerals. The gradual increase of ΔT with increasing λ_w , or equivalently, decreasing of BE concentration, in the present study may be the result of this competition; for example, when the BE concentration is relatively large (i.e., λ_w near 80 vol%), both effects may be almost the same, but the inhibition effect may become smaller at smaller BE concentrations (i.e., $\lambda_w > 90$ vol%).

3.3. Effects of Sediments on the Thickness of the Bottom of the Hydrate Stability Zone

[33] In the present study, we found that the conditions in sediments inhibit the formation of CH₄ hydrates. In our experiments, the hydrates likely formed by the following sequence. First, hydrates form at the interface between gas and the water in the largest pores. The size of the largest pores with water depends on water content of the sample. Then the hydrate grows into the smaller pore spaces. If the growth process of gas hydrates under natural conditions is the same as the process argued here, the gas hydrate stability zone should depend on the sediment conditions. Clennell *et al.* [1999] provided a conceptual model for predicting the equilibrium conditions within fine-grained sediments. The model includes reduced pore water activity in the vicinity of hydrophilic mineral surfaces and an excess internal energy

of small crystals confined in pores. They found that the growth forms commonly observed in hydrate samples recovered from marine sediments could largely be explained by capillary effects, although the kinetics of nucleation and growth were also shown to be important. Kleinberg *et al.* [2003] used nuclear magnetic resonance to study CH₄ hydrate-bearing sandstones prepared in natural conditions. They found that pore spaces up to 10 μm in diameter were saturated with CH₄ hydrates, although the measurements were limited to pore spaces exceeding 0.5 μm . Their results also suggested that CH₄ hydrates were primarily the pore-filling growth habit, and that the silica surfaces were wet by liquid water despite the hydrates in the center of the pores. We now compare the present experimental findings to the natural conditions in deep-sea sediments and the conditions under permafrost layers.

[34] We used the present results to estimate the shift of BGHS at Blake Ridge, ODP Leg 164 site 997. We use the temperature profile from Ruppel [1997] and assume that the growth habit of gas hydrates in the sediments were pore-filling with growth processes similar to those observed in the experiments of $S_w = 10$ vol%. The equilibrium temperature shifts of CH₄ hydrate in coarse-particle sediments, such as TS and BS, are approximately -0.2 K, whereas those in fine-particle sediments, such as KA and intergrain hydrates in BE, are approximately -1.1 K. Applying these results to the temperature profile in Blake Ridge, we find that the depth of BGHS is about 5 m shallower in coarse-particle sediments and about 30 m shallower in fine-particle sediments (Figure 11). This is consistent with the discrepancies between the estimated BGHS and the observed BSR at the Blake Ridge, and thus the results obtained in the present study support the conclusions of Ruppel [1997]; in particular, the best explanation of the depth offset observed at Blake Ridge is the inhibition influence on hydrate stability due to the strong capillary forces in the fine-grained sediments. Furthermore, the inhibition effects of sediments on the gas hydrates are strongly dependent on the growth habit of the hydrate in the sediments; therefore we need to better understand the formation process of gas hydrates *in situ*. It is also noticeable, as pointed out by Clennell *et al.* [1999] and Henry *et al.* [1999], that for this kind of experiment to be realistic, the sediment matrix should be subjected to a confined stress. Careful comparisons of experimental results obtained from these laboratory studies and *in situ* conditions, such as those reported by Kleinberg *et al.* [2003], will reveal the detailed effects of confined stress on the equilibrium condition shift.

4. Summary

[35] We found that the three-phase equilibrium conditions of methane hydrates in porous and sedimentary materials depended mainly on the pore size distribution in the material. Sediment samples were silica sand, sandstone, and two types of clays having different water absorption properties, materials that are typical for sediments that contain hydrate. The results from these materials were also compared with those from uniform-size glass beads having similar particle sizes as the sediment samples. These comparisons of natural and artificial samples at various water content conditions revealed the effective parameters for

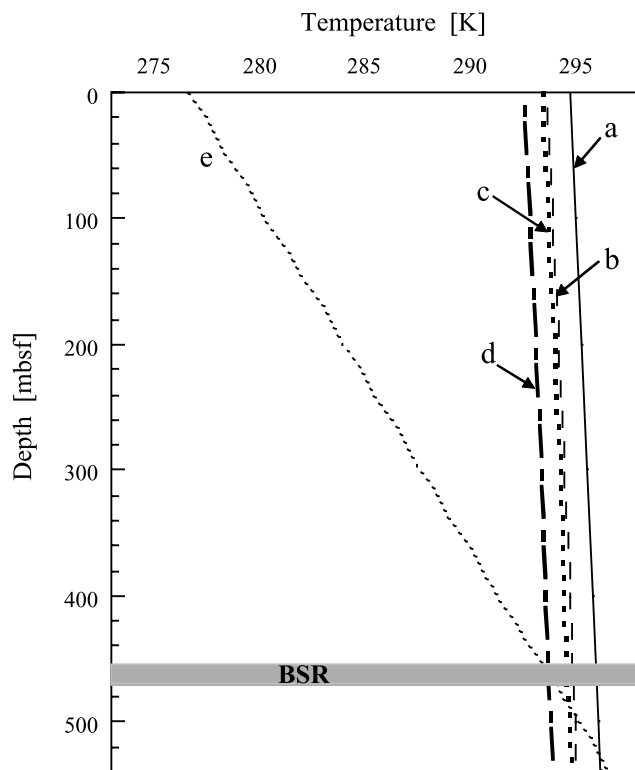


Figure 11. Comparison of the depth of BSR with the estimated depths of BGHS for several decomposition conditions of CH₄ hydrates. The solid line (“a”) represents bulk hydrate forming conditions. The dashed line (“b”) represents bulk hydrates with electrolytes [Ruppel, 1997]. The thick dotted line (“c”) is for hydrates in coarse sediments, and the thick dash-dotted line (“d”) is for hydrates in fine sediments. The fine dotted line with the smallest slope (“e”) is the temperature profile based on conditions in Blake Ridge, ODP Leg 164 Site 997 [Ruppel, 1997].

determining the equilibrium conditions for gas hydrates in natural sediments.

[36] The pore space size was found to be an important parameter. This parameter depends on the particle size and water content of the sediment. The hydrate first forms in the largest pores that are saturated with water because such water can interact with methane gas to form hydrate. Hydrate growth is inhibited when the growth occurs in small pores with the smaller the pore, the greater the inhibition. For the materials having little to no swelling when in contact with water, analysis of their data indicated that CH₄ hydrates formed between the particles and the decomposition temperature was shifted by at most -2.0 K. The maximum pore sizes that produced a temperature shift at the decomposition pressure were about $50\ \mu\text{m}$ for sand, sandstone, and $100\text{-}\mu\text{m}$ glass beads, about $10\ \mu\text{m}$ for $20\text{-}\mu\text{m}$ glass beads, and about $1\ \mu\text{m}$ for kaoline.

[37] We found that variations in the surface texture of mineral particles, specifically, the differences in surface texture among sand, clay, and glass beads, did not significantly affect the equilibrium conditions of gas hydrates formed in the pore spaces between the particles. Therefore

glass beads are expected to be a useful, well characterized material for investigating the equilibrium conditions of natural sediments having small water swelling abilities. However, when substituting sediment with glass beads, the particle size distributions should be similar because the particle size is an important effect on the temperature shift. Similar results were observed in sandstone and silica sand that had different pore sizes. This finding might have resulted from the difficulty of gas hydrate formation in such small spaces during the duration of our experiments.

[38] In clay minerals that have a relatively large amount of swelling when kept in contact with water, such as montmorillonite, the decomposition process involved two steps. The decomposition point at the higher temperature was related to the decomposition of gas hydrates formed between the clay particles, whereas the decomposition point at the lower temperature was inferred to arise from decomposition of hydrates in the clay interlayers. The decomposition-temperature shifts of these interlayer hydrates were also dependent on the initial water content, which indicates that the decomposition is controlled by the thickness of the hydrate layers between the molecular plates of the mineral. Moreover, this thickness is influenced by the swelling. In addition, the surface texture of montmorillonite molecular plates also appeared to have a thermodynamic promotion effect when bentonite was dissolved in water. However, the effect increased the equilibrium temperature at a given pressure by only about $+0.5$ K, which is much smaller than that reported previously [Cha *et al.*, 1988].

[39] Differences in the composition of the materials seemed to affect the dependence of the equilibrium temperature shift on the pore size. The most sensitive dependence on pore size occurred in kaoline, and the weakest occurs in porous glass. This difference might be caused by the stronger interactions between water molecules and clay minerals compared with those between water molecules and silica glass.

[40] With the assumption that the growth habits of gas hydrates in natural conditions are similar to those observed in the present study, we used the present results to estimate the effect that each sediment type has on the depth of BGHS. Our estimates were shown to be consistent with the experimental offset of the BGHS and BSR observed in Blake Ridge.

Notation

d_p	mode diameter of the pore distribution, μm .
d_{max}	the diameter of the largest pores that are saturated with water or with hydrates, μm .
m_b	mass of dry porous media, g.
m_w	mass of water added to the sample, g.
v_b	specific pore volume of dry porous media, $\text{cm}^3\ \text{g}^{-1}$.
P_d	measured decomposition pressure, Pa.
S_w	pore water saturation, %.
T_d	measured decomposition temperature, K.
T_e	decomposition temperature of bulk methane hydrate at P_d , K.
V_b	bulk volume of dry porous media, cm^3 .
V_w	volume of water added to the sample, cm^3 .
λ_w	volumetric water content, %.
ρ_b	bulk density of dry porous media, $\text{g}\ \text{cm}^{-3}$.

ρ_p specific porosity of dry porous media.
 ρ_w density of water, g cm⁻³.

[41] **Acknowledgments.** This work was partially supported by the Research Consortium for Methane Hydrate Resources in Japan (MH21 Research Consortium) organized by the Japan Oil, Gas and Metals National Corporation, and by the Global Environmental Research Fund organized by the Ministry of the Environment. We also acknowledged Dr. W. Shimada, Mr. S. Jin and Ms. J. Hayashi for their experimental support.

References

- Anderson, R., M. Llamedo, B. Tohidi, and R. W. Burgass (2003a), Characteristics of clathrate hydrate equilibria in mesopores and interpretation of experimental data, *J. Phys. Chem. B*, *107*, 3500–3506.
- Anderson, R., M. Llamedo, B. Tohidi, and R. W. Burgass (2003b), Experimental measurement of methane and carbon dioxide clathrate hydrate equilibria in mesoporous silica, *J. Phys. Chem. B*, *107*, 3507–3514.
- Cha, S. B., H. Ouar, T. R. Wildeman, and E. D. Sloan Jr. (1988), A third-surface effect on hydrate formation, *J. Phys. Chem.*, *92*, 6492–6494.
- Chuvilin, E. M., E. V. Perlova, N. A. Makhonina, V. S. Yakushev, and D. V. Dubinyak (2002), Peculiarities of methane hydrate formation/dissociation P/T conditions in sediments of different composition, *Proc. 4th Int. Conf. On Gas Hydrates*, pp. 734–739, Int. Sci. Comm. of ICGH-4, Yokohama, Japan.
- Clennell, M. B., M. Hovland, J. S. Booth, P. Henry, and W. J. Winters (1999), Formation of natural gas hydrates in marine sediments: 1. Conceptual model of gas hydrate growth conditioned by host sediment properties, *J. Geophys. Res.*, *104*, 22,985–23,003.
- Englezos, P., and S. Hall (1994), Phase equilibrium data on carbon dioxide hydrate in the presence of electrolytes, water soluble polymers and montmorillonite, *Can. J. Chem. Eng.*, *72*, 887–893.
- Guggenheim, S., and A. F. Koster van Groos (2003), New gas-hydrate phase: Synthesis and stability of clay-methane hydrate intercalate, *Geology*, *31*, 653–656.
- Handa, Y. P., and D. Stupin (1992), Thermodynamic properties and dissociation characteristics of methane and propane hydrates in 70–Å-radius silica gel pores, *J. Phys. Chem.*, *96*, 8599–9603.
- Henry, P., M. Thomas, and M. B. Clennell (1999), Formation of natural gas hydrates in marine sediments: 2. Thermodynamic calculations of stability conditions in porous sediments, *J. Geophys. Res.*, *104*, 23,005–23,022.
- Kleinberg, R. L., C. Flaum, D. D. Griffin, P. G. Brewer, G. E. Malby, E. T. Peltzer, and J. P. Yesinowski (2003), Deep sea NMR: Methane hydrate growth habit in porous media and its relationship to hydraulic permeability, deposit accumulation, and submarine slope stability, *J. Geophys. Res.*, *108*(B10), 2508, doi:10.1029/2003JB002389.
- Kotkoskie, T. S., B. Al-Ubaldi, T. R. Wildeman, and E. D. Sloan (1992), Inhibition of gas hydrates in water-based drilling muds, *SPE Drill. Eng.*, *130*–136.
- Lee, K. M., H. Lee, J. Lee, and J. M. Kang (2002), CO₂ hydrate behavior in the deep ocean sediments: Phase equilibrium, formation kinetics, and solubility, *Geophys. Res. Lett.*, *29*(21), 2034, doi:10.1029/2002GL015069.
- Makogon, Y. F. (1974), *Hydrates of Natural Gas* (in Russian), 208 pp., Nedra, Moscow Russia.
- Makogon, Y. F. (1981), *Hydrates of Natural Gas*, translated from Russian by W. J. Cieslesicz, 237 pp., PennWell, Tulsa, Okla.
- Matsumoto, R., Y. Watanabe, M. Satoh, H. Okada, Y. Hiroki, M. Kawasaki, and ODP Leg 164 shipboard scientific party (1996), Distribution and occurrence of marine gas hydrates—Preliminary results of ODP Leg 164: Blake Ridge Drilling (in Japanese), *J. Geol. Soc. Jpn.*, *102*, 932–944.
- Ostergaard, K. K., R. Anderson, M. Llamedo, and B. Tohidi (2002), Hydrate phase equilibria in porous media: Effect of pore size and salinity, *Terra Nova*, *14*, 307–312.
- Ouar, H., S. B. Cha, T. R. Wildeman, and E. D. Sloan (1992), The formation of natural gas hydrates in water-based drilling fluids, *Chem. Eng. Res. Des.*, *70*, 48–54.
- Park, S.-H., and G. Sposito (2003), Do montmorillonite surfaces promote methane hydrate formation? Monte Carlo and Molecular dynamics simulations, *J. Phys. Chem. B*, *107*, 2281–2290.
- Ruppel, C. (1997), Anomalously cold temperature observed at the base of the gas hydrate stability zone on the U.S. Atlantic passive margin, *Geology*, *25*, 699–702.
- Sloan, E. D., Jr. (1998), *Clathrate Hydrates of Natural Gases*, 2nd ed., 705 pp., Marcel Dekker, New York.
- Smirnov, K. S., and D. Bougeard (1999), A molecular dynamics study of structure and short-time dynamics of water in Kaolinite, *J. Phys. Chem. B*, *103*, 5266–5273.
- Smith, D. H., J. W. Wilder, and K. Seshadri (2002), Methane Hydrate Equilibria in Silica Gels with Broad Pore-Size Distributions, *AIChE J.*, *48*, 393–400.
- Starobinets, I. S., and R. N. Murogova (1985), Trapping and conducting role of cryolithozone rocks in relation to migrating hydrocarbons (in Russian), *Geology Oil Gas*, *NI*, 24–27.
- Uchida, T., T. Ebinuma, and T. Ishizaki (1999), Dissociation condition measurements of methane hydrate in confined small pores of porous glass, *J. Phys. Chem. B*, *103*, 3659–3662.
- Uchida, T., T. Ebinuma, S. Takeya, J. Nagao, and H. Narita (2002), Effects of pore sizes on dissociation temperatures and pressures of methane, carbon dioxide and propane hydrate in porous media, *J. Phys. Chem. B*, *106*, 820–826.
- Van der Waals, J. H., and J. C. Platteeuw (1959), Clathrate solutions, *Adv. Chem. Phys.*, *2*, 1–57.
- Wilder, J. W., K. Seshadri, and D. H. Smith (2001), Modeling hydrate formation in media with broad pore size distributions, *Langmuir*, *17*, 6729–6735.
- Yakushev, V. S. (1990), Peculiarities of mass-exchange in dispersed rocks during hydrate formation, in *Natural and Technogenic Gas Hydrates* (in Russian), edited by A. I. Gritsenko and V. A. Istomin, pp. 174–187, VNIIGAZ, Moscow.

T. Uchida, Department of Applied Physics, Graduate School of Engineering, Hokkaido University, Sapporo, 060-8628, Japan. (t-uchida@eng.hokudai.ac.jp)

E. M. Chuvilin, T. Ebinuma, R. Ohmura, H. Minagawa, J. Nagao, H. Narita, and S. Takeya, Institute for Energy Utilization, AIST, Sapporo, 062-8517 Japan.

V. A. Istomin and V. S. Yakushev, All Russian Research Institute of Natural Gases (VNIIGAZ), 142717, Moscow, Russia.